Structural and molecular determinants affecting the interaction of retinol with human CRBP1

STRUCTURAL AND MOLECULAR DETERMINANTS AFFECTING THE INTERACTION OF RETINOL WITH HUMAN CRBP1

Ilaria Menozzi [a,b §], Francesca Vallese [c §], Eugenia Polverini [b], Claudia Folli [d], Rodolfo Berni [a]* and Giuseppe Zanotti [c]*

[a] Department of Life Sciences, University of Parma, Parco Area delle Scienze 23/A, 43124 Parma, Italy

[b] Department of Physics and Earth Sciences, University of Parma, Parco Area delle Scienze 23/A, 43124 Parma, Italy

[c] Department of Biomedical Sciences, University of Padua, Via Ugo Bassi 58/B, 35131 Padua, Italy

[d] Department of Food Sciences, University of Parma, Parco Area delle Scienze 23/A, 43124 Parma, Italy

[§] Both authors contributed equally to this work

*To whom correspondence should be addressed:

Giuseppe Zanotti, Department of Biomedical Sciences, University of Padua, Via Ugo Bassi 58/B, 35131 Padova, Italy Tel.: +39 049 8276409, Fax + 39 049 8073310; email: giuseppe.zanotti@unipd.it;

Rodolfo Berni, Department of Life Sciences, University of Parma, Parco Area delle Scienze 23/A, 43124 Parma, Italy. Tel: +39 0521 905645, Fax +39 0521 905151; email: rodolfo.berni@unipr.it

Running Title: Determinants for retinol-CRBP1 interactions

Abbreviations used: CRBP, cellular retinol-binding protein; iLBPs, intracellular lipid-binding proteins; CRABPs, cellular retinoic acid-binding proteins; FABPs, fatty acid-binding proteins; HT, His-Tag; PDB, Protein Data Bank; RMSD, root mean square deviation; RMSF, root mean square fluctuation; MD, molecular dynamics; PCR, Polymerase Chain Reaction.

ABSTRACT

Four cellular retinol-binding protein (CRBP) types (CRBP1,2,3,4) are encoded in the human genome. Here, we report on X-ray analyses of human apo- and holo-CRBP1, showing nearly identical structures, at variance with the results of a recent study on the same proteins containing a His-Tag, which appears to be responsible for a destabilizing effect on the apoprotein. The analysis of crystallographic B-factors for our structures indicates that the putative portal region, in particular α-helix-II, along with Arg58 and the E-F loop, is the most flexible part of both apo- and holoprotein, consistent with its role in ligand uptake and release. Fluorometric titrations of wild type and mutant forms of apo-CRBP1, coupled with X-ray analyses, provided insight into structural and molecular determinants for the interaction of retinol with CRBP1. An approximately stoichiometric binding of retinol to wild type apo-CRBP1 (Kd ~ 4.5 nM), significantly lower binding affinity for both mutants Q108L (Kd ~ 65 nM) and K40L (Kd ~ 70 nM) and very low binding affinity for the double mutant Q108L/K40L (Kd ~ 250 nM) were determined, respectively. Overall, our data indicate that the extensive apolar interactions between the ligand and hydrophobic residues lining the retinol binding cavity are sufficient to keep it in its position bound to CRBP1. However, polar interactions of the retinol hydroxyl end group with Gln108 and Lys40 play a key role to induce a high binding affinity and specificity for the interaction.

Keywords: vitamin A, retinoid-binding proteins, intracellular lipid-binding proteins, mutational analyses, molecular dynamics simulation

INTRODUCTION

Vitamin A fulfils essential roles in the physiology of vertebrates, being involved in cell growth and differentiation, reproduction, embryonic development, and vision. Retinol, the alcoholic form of vitamin A, one among several other forms of this vitamin, achieves a drastically higher chemical stability when it is bound to serum retinol-binding protein (RBP 4) and intracellular retinol-binding proteins (CRBPs). In addition to this chaperoning role, the interaction with retinol-binding proteins permits the solubilization in the aqueous medium of the highly hydrophobic retinol molecule. Four homologous CRBPs (CRBP1, 2, 3 and 4), encoded in the human genome and well represented in other mammals, are believed to be the intracellular carriers for all-*trans* retinol (Folli et al., 2001; 2002). CRBPs belong to a superfamily of small cytoplasmic proteins that interact specifically with hydrophobic ligands, the intracellular lipid-binding proteins (iLBPs). Besides CRBPs, well-characterized members of the iLBP superfamily are the cellular retinoic acid-binding proteins (CRABPs) and the fatty acid-binding proteins (FABPs) (Schaap et al., 2002; Smathers and Petersen, 2011). Although members of the different protein families may possess a low sequence identity, a basic structural motif has been found for the different iLBPs characterized thus far. In all these proteins, 10 β-strands (A-J) and two α-helices (I and II) fold to form a well-defined barrel, whose internal cavity represents the binding site for hydrophobic ligands. It has been suggested that the portal region for the ligand comprises α-helix II and CD- and EF-loops (Hodsdon and Cistola, 1997; Lu et al., 2000) (Franzoni et al., 2002).

X-ray analyses of holo-CRBP1 and holo-CRBP2 have previously shown that the two conserved residues Gln108 and Lys40 are in close proximity with the retinol hydroxyl end group, suggesting their critical role in the interaction with the ligand ((COWAN et al., 1993), (WINTER et al., 1993)). With regard to its functional properties, CRBP1 possesses very high affinity for retinol, with K_d values in the nanomolar or sub-nanomolar range (Malpeli et al., 1995; Ong et al., 1994). The results of *in vitro* studies have indicated that the formation of the CRBP1-retinol complex may be functional for several processes and reactions, such as retinol exchange through cell membrane mediated by Stra6 (Kawaguchi et al., 2012), retinol esterification (HERR and Ong, 1992; Ong et al., 1988; YOST et al., 1988), retinyl ester hydrolysis (BOERMAN and NAPOLI, 1991; Ottonello et al., 1987), and oxidation of retinol to retinal, a key step of retinoic acid biosynthesis (Ottonello et al., 1993) (Boerman and NAPOLI, 1996). Although a high binding affinity for retinol, with K_d values in the nanomolar range, was also established for CRBP2 (Ong et al., 1994) (Nossoni et al., 2014), a study that allowed a direct competition of CRBP1 and 2 suggested that the affinity of CRBP1 for retinol may be 100 fold greater than that of CRBP2

(LI et al., 1991). In addition to retinol, *in vitro* both CRBP1 and 2 can form complexes with all-*trans* retinal, which might also be serving as substrates for certain enzymatic activities. Although structural evidence has been presented to indicate that CRBP2 can establish better interactions with retinal as compared to CRBP1 (Nossoni et al., 2014), significantly lower binding affinities for retinal as compared to retinol have been found for both CRBP1 (Malpeli et al., 1995) and CRBP2 (Nossoni et al., 2014).

Recently, the X-ray structures of His-tagged apo- and holo-CRBP1 have been determined, indicating the occurrence of some conformational changes affecting the protein backbone in the putative portal region (Silvaroli et al., 2016). Here, we present for the same proteins experimental and structural evidence showing the key role played by residues Gln108 and Lys40 in the interaction of CRBP1 with retinol and structural evidence for the flexibility of the putative portal region, consistent with its role in ligand binding and release. In addition, the high resolution structural characterization of WT human apo- and holo-CRBP1 does not reveal the significant conformational differences previously observed for the His-tagged apo- and holoproteins, which are likely to be due to a destabilizing effect of the tag on the protein structure.

MATERIAL AND METHODS

Materials

all-*trans* retinol was purchased from Sigma. All other chemicals were of analytical grade.

Methods

Site-directed mutagenesis of human CRBP1

The expression vector PET28b (Novagen) containing the entire human CRBP1 coding sequence, obtained previously in our laboratory (Folli et al., 2002), was used as a template for site-directed mutagenesis. The three mutant forms K40L, Q108L, K40L/Q108L of human CRBP1 were prepared by using the Quick-Change mutagenesis protocol, which employs a high-fidelity thermostable DNA polymerase (PfuTurbo DNA polymerase; Stratagene). Mutagenic oligonucleotide primers were designed and synthesized for each single mutation: upstream primer (5'-CTTGCTGAAGCCAGACCTAGAGATCGTGCAGGAC-3') and downstream primer (5'-GTCCTGCACGATCTCTAGGTCTGGCTTCAGCAAG-3') for the K40L mutation, and upstream primer (5'-GTGGCTGGACCCTGTGGATCGAGGG-3') and downstream primer (5'-CCCTCGATCCACAGGGTCCAGCCAC-3') for the Q108L mutation. The latter primers for the Q108L mutation were also used on the K40L mutant plasmid to obtain the double K40L/Q108L

mutation. To digest the parental DNA template, the PCR products were treated with DpnI (Stratagene). Each digestion product was then used to transform E.coli XL1 Blue cells. Some colonies were chosen and sequenced to verify the occurrence of the desired mutation. Finally, E.coli BL21 (DE3) cells were transformed with mutant plasmids in order to proceed with the expression and purification of mutant proteins.

Expression and purification of WT and mutant forms of human CRBP1

The expression of WT human CRBP1 and its mutant forms was induced by adding 0.5 mM ipopropyl-1-thio-β-D-galactopyranoside to the colture of *E. coli* BL21 (DE3) cells. After incubation for 16 hours at 4°C, cells were harvested by centrifugation (for 15 min, at 7000 rpm, at 4°C), suspended in the lysis buffer (Na phosphate 50mM, NaCl 0.3 M, pH 8.0, 10% glycerol), and finally lysed by sonication, with a yield of more than 60% of soluble protein for both WT and mutant proteins. In order to obtain pure proteins, WT CRBP1 and its mutant forms were purified using a two-step procedure, consisting of anion exchange (High Q Support, BIO-RAD) and size exclusion (Ultrogel AcA54, PALL Life Sciences) chromatographies. The final yield was 7-10 mg/L of bacterial colture for WT and mutant proteins. The ε_{280} (molar extinction coefficient at 280 nm) of WT and mutant CRBP1 was estimated to be 26595 M^{-1} cm^{-1} on the basis of amino acid sequences. To obtain an authentic apoprotein from purified recombinant WT CRBP1, the protein was delipidated by treatment with the hydrophobic resin Hydroxyalkoxypropyl-Dextran Type IX (Sigma Aldrich), equivalent to Lipidex 1000, essentially as described (Glatz and Veerkamp, 1983).

Binding of retinol to WT and mutant forms of CRBP1

Absorption spectra of WT and mutant forms of CRBP1 in complex with retinol were obtained upon addition of a slight molar excess of all-*trans* retinol (dissolved in ethanol) to 7.5 μM recombinant WT and mutant forms of CRBP1, in 50 mM Tris HCl, 0.15 M NaCl, pH 7.5. Fluorometric binding assays for WT and mutant forms of CRBP1 (protein concentration 0.6-0.7 μM) were carried out, by means of a PerkinElmer LS-50B fluorimeter, by monitoring the quenching of the intrinsic protein fluorescence (excitation and emission at 280 and 330 nm, respectively) upon addition of small aliquots (0.2-0.4 μL) of stock solutions of all-trans-retinol in ethanol ($\varepsilon_{325\ nm}$ = 46000 M^{-1} cm^{-1}) directly into the fluorometer cuvette,. After each addition, the protein solution was stirred gently and allowed to equilibrate at 20°C in the dark for a few minutes before measuring the fluorescence intensity. Binding data, obtained in triplicate for each CRBP1 form, were analyzed by nonlinear regression of experimental data as described previously (Malpeli et al., 1995), using Sigma Plot software (Jandel, Corte Madera, CA).

Crystallization and structure determination

Crystals of WT human apo and holo CRBP1 and of the mutant forms of human CRBP1 (apo- and holo CRBP1 K40L, holo CRBP1 Q108L and holo CRBP1 K40L/Q108L), were obtained at room temperature using the hanging-drop technique from a precipitant solution containing 0.2 M ammonium chloride, 0.1 M sodium acetate, pH 5,0, 20% PEG 6000 (PACT 1-8, Molecular Dimensions, UK), a condition that is similar, in regard to both pH and precipitant, to that adopted for the crystallization of HT human CRBP1 (Silvaroli et al., 2016). Crystals diffracted at high resolution, from 1.23Å to 1.43Å resolution, except for WT apo CRBP1, which diffracted to a relatively lower resolution, 1.70 Å. X-ray diffraction data were collected at the beamline PXIII (SLS synchrotron, Switzerland), ID29 (ESRF, Grenoble, France) or ID30B at 100°K, without any cryoprotectant. Data were processed by XDS (Kabsch, 2010) and scaled with Scala (Evans, 2006). All crystals belong to the $P2_12_12_1$ space group, with unit cell dimensions reported in Table I. The V_M value for all crystals is 2.00 - 2.08 $Å^3$/Da, corresponding to a solvent content of about 38%-41% of the total volume, with one molecule in the asymmetric unit. The structure was solved by molecular replacement with software Molrep (Lebedev et al., 2007), using as template the solution structure 1KGL (Franzoni et al., 2002). The structures were refined using Refmac5 (Murshudov et al., 2011) or Phenix (Adams et al., 2010) and manually rebuilt and corrected by software Coot (Emsley and Cowtan, 2004). Towards the end of the refinement, the electron density for the retinol or a different ligand bound inside the cavity was clearly visible in all cases, except for the authentic apo CRBP1 and apo CRBP1 K40L (which were devoid of any ligand), and was included with restraints produced by server PRODRG (Schuttelkopf and van Aalten, 2004). Solvent molecules were added automatically using the Phenix automated procedure and checked manually. Hydrogen atoms were introduced in the last cycle of refinement. The statistics of data collection and refinement are reported in Table I. The geometry of the final model was checked by Molprobity (Lovell et al., 2003).

Molecular Dynamics simulations

Molecular dynamics (MD) simulations were performed by adding a His_6-Tag to the WT apo CRBP1 crystal structure by means of the Swiss-PDB Viewer program (Guex and Peitsch, 1997). To better reproduce the acidic crystallization conditions (pH 5.5) of HT human CRBP1 (Silvaroli et al., 2016), the pKa values of ionizable residues were calculated by means of the program PROPKA, embedded in the software package PDB2PQR (Dolinsky et al., 2004)). Based on PROPKA results, a first MD simulation was carried out on the His-tagged protein, keeping all His

residues in a protonated form. Subsequently, to discriminate the effects of the charges of protonated His-residues, a second MD simulation was performed with all His residues in their neutral form. Moreover, a control MD simulation on the WT apo-CRBP1 itself was carried out.
MD simulations were carried out using the GROMACS (4.5.5) software package (van der Spoel et al., 2005) with the Gromos ffG53a6 force-field (Oostenbrink et al., 2004). In all the dynamics simulations, the protein structure was embedded in a water box extending 10 Å around it and Na and Cl counterions were added to assure the neutrality of the system and to reach the physiological salt concentration of 150 mM. The whole system was subjected to an energy minimization and then a position restrained MD, lasting 50 ps, was performed to relax the solvent around the protein. Finally a 100 ns full MD run was carried on, at 300 K and 1 atm. The analyses of the trajectories were performed by means of the VMD software (Humphrey et al., 1996).

Databases. Structural data factors are available in the Protein Data Bank under the accession numbers: 5LJB (holo CRBP1), 5LJC (holo CRBP1/Q108L), 5LJD (holo CRBP1/K40L), 5LJE (holo CRBP1/K40L,Q108L), 5LJG (fatty acid bound CRBP1), 5LJH (apo CRBP1/K40L mutant), 5LJK (apo CRBP1).

RESULTS

Structures of human Wild Type (WT) apo and holo CRBP1

Our data on the structures of human WT CRBP1, as well as its mutant forms, were obtained before the recent publication dealing with the structure of the same human protein, which, differently from our protein, contained a His_6-Tag at its C-terminus (Silvaroli et al., 2016), and is designated in this work as His-Tag (HT) CRBP1. Despite this difference, WT and mutant forms of CRBP1 (see below) and HT CRBP1 crystallize in similar conditions (see Materials and Methods) and crystals are essentially isomorphous **(Table I),** with the exception of HT apo CRBP1 (Silvaroli et al., 2016)**.**

All residues present in the structures of WT CRBP1, from Pro1 to Gln134, have been included in our structural models. They are clearly visible in the electron densities, except for Pro1, which is partially flexible. The root mean square deviation (RMSD) for the superposition of equivalent Cα atoms of human WT holo CRBP1 and human HT holo CRBP1 (PDB ID 5H8T, (Silvaroli et al., 2016)) is 0.55 Å. The main difference between the two proteins is at the C-terminus, where the presence of the His-Tag influences the conformation of the last three amino

acids. The RMSD is 0.793Å for the comparison of the structures of human WT holo CRBP1 and rat WT holo CRBP1 (PDB ID 1CRB, [8]), but the latter difference must be essentially ascribed to the lower resolution of the previous structure and possibly to different crystallization conditions. In WT holo CRBP1, the protein structure and the mode of binding of retinol in the inner cavity is the same as that found for HT holo CRBP1, with the retinol hydroxyl group pointing towards Gln108 and Lys40 and forming H-bonds with both Oε1 atom of Gln108(OH – Oε1 distance, 2.92Å) and Nζ of Lys40 (OH – Nζ distance, 3.22 Å), respectively (the same distances are 2.81 Å and 2.95 Å, respectively, for HT holo CRBP1 (Silvaroli et al., 2016)) (**Figs. 1A and 2A)**

Unexpectedly, in a first structure of the putative WT apo CRBP1, crystallized in the same conditions as the holo-protein and in the absence of any added ligand, a long linear electron density, slightly bent, was visible inside the binding cavity (**Fig. 1B),** which indicates that upon its expression the protein bound an as-yet-uncharacterized compound produced by *E. coli* metabolism and possessing affinity for CRBP1. A saturated fatty acid was selected as a possible hydrophobic ligand, since the flexibility of its chain would allow a better fitting in the density. A palmitate molecule fitted quite well in the electron density, with an occupancy slightly lower than 1. The RMSD for the superposition of the equivalent Cα atoms of WT holo CRBP1 and WT CRBP1 in complex with the hypothetical ligand is 0.16 Å, with the positions of all the side chains pointing inside the cavity perfectly conserved, in keeping with the rigidity of the protein scaffold. In our model, one of the oxygen atoms of the carboxylate group of the hypothetical fatty acid interacts with nitrogen of Lys40 (O2 – Nζ, 2.71Å) and with a water molecule (O2 – O, 2.72Å), the second with the oxygen of Gln108 (O1 – Oε1, 2.86Å) (**Fig. 2D**). It is also very likely that an ionic interaction takes place between the positively charged $–NH_3^+$ group of Lys40 and the negatively charged carboxylate of the hypothetical fatty acid.

The latter observations suggested to us that the mutation K40L would lead to a lack of interaction between the ε-amino group of Lys40 and the carboxylate group of the aforementioned hypothetical ligand, with the possibility of generating an authentic apo CRBP. Indeed, upon crystallization the X-ray analysis of the K40L CRBP1 mutant form revealed that it was a real apo-protein, in which the cavity was filled with 11 solvent molecules that do not mimic the position of the hypothetical ligand. This result is consistent with our hypothesis that CRBP1 has the ability to bind carboxylic acids, such as fatty acids, through the formation of an ionic bond with Lys40. The latter ligand, however, does not possess high binding affinity for CRBP1, since it can be easily and fully displaced by the retinol.

In order to determine the structure of an authentic WT apo CRBP1, the WT CRBP1 obtained upon expression in *E. coli* was delipidated by treatment with a hydrophobic resin (see

Material and Methods) and crystallized. The structures of WT apo CRBP1 and apo CRBP1 K40L are nearly superimposable, the RMSD for the superposition of equivalent Cα atoms being 0.29 Å **(Fig. 1 C).** The structures of WT apo CRBP1 is at lower resolution (1.7Å) as compared to the HT apo CRBP1. Despite that, most of the solvent molecules located inside the cavity are conserved in both structures, as well as in the case of the structure of apo CRBP1 K40L mutant form. The RMSD for equivalent Cα atoms upon superposition of WT apo CRBP1 and HT apo CRBP1 is higher, 0.85Å. In particular, we do not observe for our WT apo-CRBP1 the movement of the E-F loop (residues 73-81), which by itself shows a RMSD of 3.05 Å in the comparison between WT and HT apo CRBP1, and of the nearby side chain of Tyr60, found for the HT apo-CRBP1. On the contrary, the latter region of WT apo-CRBP1 maintains essentially the conformation found for WT and HT holoproteins. In fact, WT holo and apo CRBP1 are very similar, the RMSD for the superposition of the equivalent Cα atoms being 0.21Å **(Fig. 1 C)**. The positions of all the side chains pointing inside the cavity are perfectly conserved, a clear indication of the rigidity of the protein scaffold. The C-terminus also points in the same way as the holoprotein.

By means of a 100 ns molecular dynamics (MD) simulation, we have analyzed the effect of the presence of the His-Tag on the WT apo CRBP structure, possibly responsible for protein conformational changes. To this end, a His_6-Tag was added to the WT apo-CRBP structure. To better reproduce the acidic experimental conditions, the pKa values of the ionizable residues were calculated taking into account the local structural environment (see Materials and Methods). As a result, at the crystallization condition of pH 5.5, all the His residues are likely to be mostly protonated. Therefore, a MD simulation was performed on the His-tagged structure with all the His residues in a charged state. Nevertheless, to exclude that the charge of His-residues was the main cause of any enhanced mobility of the protein, a second MD simulation was carried out in the same conditions but with all the His residues in the unprotonated form. Finally, a simulation on the WT apo-CRBP structure without the His-Tag was also carried out as a control. From the plot of the root mean square fluctuation (RMSF) of Cα atoms (calculated on the last 70 ns of simulation, during which the protein had already achieved a stable structure), we can clearly see that the His-Tagged structure in both cases shows a flexibility greater than that of the WT control, especially affecting the portal region (**Fig. 3**). The higher flexibility of the His-Tagged structure is confirmed by the analysis of B-factors: the HT apo CRBP1 structure (Silvaroli et al., 2016) shows clearly higher values for the whole portal region as compared to the WT apo CRBP1 (**Supplemental Data, Fig. 1**).

Structures of mutant forms (K40L, Q108L and K40L/Q108L) of human holo CRBP1.

The structures of the holo mutant forms Q108L, K40L and K40L/Q108L of human CRBP1 are very similar to that of WT holo CRBP1 (**Fig. 1C**), indicating that the presence of a Leu at position 40 and/or 108 does not minimally perturb the protein barrel that hosts the ligand. In fact, the RMSD for the superposition of the equivalent Cα atoms of WT holo CRBP1 with those of the holo mutant forms Q108L, K40L and K40L/Q108L are 0.16 Å, 0.41Å and 0.29Å, respectively.

As mentioned above, in WT holo CRBP1 the retinol hydroxyl end group is bound in the inner part of the cavity and it forms two H-bonds, with Gln108 and Lys40. In the holo mutant forms the retinol is positioned in the inner protein cavity, occupying the same position as in the case of WT holo CRBP1. In the K40L mutant form, the retinol hydroxyl end group points towards Gln108, as in the WT protein, forming a H bond with its oxygen atom (OH – Oε1 distance 2.41Å, **Fig. 2B**). In the Q108L mutant form, the hydroxyl group is less defined, but still visible, in the electron density, since it is present in two alternate conformations: in one it points towards Met62 (O – Sδ62 distance, 2.77Å) and in the other it points towards Lys40 (O – Nζ40 distance, 2.57Å) (**Fig. 2C**). In the double mutant form K40L/Q108L, the density for the retinol moiety -CH_2-OH is not visible, indicating that this end portion of the ligand is mobile, due to the lack of any anchor for the -OH group.

Thermal motions

The analysis of B-factors for the various structures we have determined is significant, since it clearly indicates that the α-helix-II, along with EF-loop and Arg58 (CD-loop), is the most flexible part of the protein, even in WT holo CRBP1 (**Fig. 4)**. This flexibility is increased in the presence of the different mutations for the holo-proteins, and in some cases it also propagates to the first helix and to some loops. The comparison of holo- and apo- WT CRBP1 (**Fig. 4** A and E, respectively) and of holo- and apo CRBP1 K40L (**Fig. 4** B and F, respectively) indicates that the absence of the ligand inside the cavity somehow further influences the flexibility of the protein, and in particular increases the mobility of the α-helix-II.

Binding assays for the interaction of retinol with mutant forms of human WT apo CRBP1

The binding of retinol to WT and mutant forms of human apo CRBP1 was analyzed by monitoring the formation of typical absorption spectra of the bound ligand, which in the case of the WT protein (**Fig. 5 A**) is characterized by a peak at approx. 348 nm, with two shoulders at 333 and 365 nm, respectively. In the case of the holo Q108L CRBP1 (**Fig. 5 B)**, a similar absorption spectrum is obtained, while in the case of the holo K40L CRBP1 (**Fig. 5 C)** the absorption spectrum shows three better defined peaks at 330, 345 and 363nm, respectively. When compared to the peaks

of the holo K40L CRBP1, three similar absorption peaks, although with lower intensity, are also visible for the double mutant holo K40L/Q108L (**Fig. 5 D)**. The lower absorption intensities for the latter mutant form are attributable to a relatively lower saturation by the chromophoric ligand, due to the low binding affinity.The aforementioned results suggest that the presence of Lys40 and its interaction with retinol are critical for determining the characteristic chromophoric properties of the CRBP1-bound retinol, which are likely due to the proximity of the presumably protonated side chain of Lys40 to the retinol isoprene tail (COWAN et al., 1993; Franzoni et al., 2002). Spectrofluorometric titrations of WT and mutant forms of apo CRBPI with retinol were carried out to determine the dissociation constant of the retinol-protein complexes, by exploiting the quenching of the intrinsic protein fluorescence, which is associated with retinol binding to the apoprotein as a result of an efficient energy transfer to the chromophoric protein-bound ligand (**Fig. 5**). Similar Kd values could be estimated for the two single mutants Q108L (65 ± 5 nM) and K40L (70 ± 5 nM), which are much higher than that determined for WT CRBP1 (4.5 ± 0.5 nM). In the case of the double mutant K40L/Q108L CRBP1, the estimated Kd value is approx. 250 nM (250 ± 30 nM), indicating that the substitution of both key residues results in a further strong decrease in binding affinity.

DISCUSSION

The interactions of retinol bound inside the cavity of the various forms, WT and mutant, of CRBP1 are summarized in Table II. The retinol in all cases is bound in the same orientation, and its -OH group interacts, when possible, with Lys40 and Gln108. When Lys40 is absent, the interaction is limited to Gln108, whilst when the latter residue is absent the –OH is present in double conformation and it interacts with both Lys40 and Met62. In the K40L/Q108L double mutant, the retinol end moiety –CH2-OH is mobile and its position is not visible in the electron density, while the maintenance of the shape of the cavity appears to be sufficient to hold the ligand in its position. At the same time, the Q108L and K40L mutant forms and the Q108L/K40L double mutant form exhibit low and very low binding affinities, respectively, for the retinol molecule, as compared to WT CRBP1. Taken together, the latter data indicate that the extensive hydrophobic interactions between the ligand and hydrophobic residues lining the binding cavity are strong enough to retain the ligand, and that polar interactions of the retinol hydroxyl end group with Lys40 and Gln08 residues play a crucial role to induce a high binding affinity and binding specificity.

An apparent Kd value of about 4.5 nM has been determined here by spectrofluorometric titration for the binding of retinol to human WT CRBP1, to be compared with higher (10-20 nM, Ong et al. 1994; Silvaroli et al. 2016) and lower (2 nM, Malpeli et al., 1995) Kd values that were

determined previously for CRBP1 by using the same technique. It should be pointed out, however, that such values may represent overestimates of the Kd values, as suggested by Ong et al. (1994) and evaluated experimentally by means of competitive binding assays by Malpeli et al. (1995). In particular, the latter assays indicated that the Kd value for the binding of retinol to CRBP1 may be as low as 0.1 nM.

When the crystal structures of human WT apo and holo CRBP1 are compared, they are essentially identical. When such structures are compared with those containing a His_6-Tag (Silvaroli et al., 2016), the holo forms are highly similar, with the exception of the last residues at the C-terminus, which are influenced by the presence of the His-Tag. Instead, a striking difference between the E-F loops of the two apo forms is observed. In this respect, it should be noted that the holo crystals of HT CRBP1 and the apo and holo crystals of WT CRBP1 are nearly isomorphous, whilst the apo crystals of HT and WT CRBP1 are not, despite the fact that they belong to the same space group $P2_12_12_1$. On the contrary, crystals of WT holo, apo, and mutant forms of CRBP1 are all isomorphous. Notably, NMR studies have previously shown that the structures in solution of rat WT apo and holo CRBP1 are also highly similar (Mittag et al., 2006), in agreement with our results on the X-ray analyses of the crystal structures of human WT apo and holo CRBP1.

Regarding the difference between HT and WT apoproteins, it should be pointed out that the His-Tag tail in the crystal is close to the region 57-60, one of the two areas involved in conformational differences between holo- and apo- proteins (the distance between the imidazole ring of His140 and the closest atom of Asn59 is about 5Å, and that between His139 and the closest atom of Arg52 is less than 4 Å). In regard to this point, we could hypothesize that the destabilization of this area in HT apo CRBP1 is transmitted to the nearby 75-79 loop. This destabilization is likely to be possible due to the lack of a ligand bound inside the cavity, which by itself is able to stabilize the 3D structure in the holoprotein. On the contrary, in the absence of the ligand a less rigid protein scaffold could be destabilized by the interaction of the protein surface with the His-Tag tail. His residues are likely to be mostly protonated at the acidic pH of the crystallization medium (Silvaroli et al., 2016). However, the detection of a greater structural mobility also in the simulation with unprotonated His-residues indicates that the presence of the His positive charges is not responsible for the higher flexibility. The results of molecular dynamics simulations also reveal interactions between the His-Tag with the protein surface that lead to a destabilization of the portal region. Examples of other proteins indicating that the His-Tag may have an impact on critical properties of proteins are present in the literature ((Randolph, 2012), and references therein). Interestingly, in a previous study the high resolution crystal structures of

WT apo and holo human cellular retinoic acid binding type II (CRABPII) were found to be very similar, while the crystallization of the His_6-tagged protein resulted in poorly diffracting crystals (Vaezeslami et al., 2006).

The retinol molecule is deeply buried inside its binding cavity in CRBP1. This feature ensures the complete shield and protection of the ligand from the external environment. Since the superimposition of apo- and holo-structures of WT CRBP1 reveals for both a closed conformation and only minimal changes between them, as-yet-uncharacterized conformational changes affecting the putative portal region are expected to occur upon retinol uptake and release. The analysis of thermal motions, based on crystallographic B-factors, indicates for WT CRBP1 a high flexibility of the region comprising α-helix-II and CD- and EF-loops, especially in the case of the apoprotein. Such flexibility may account for the occurrence of transient conformational changes affecting the portal region, necessary to allow the retinol to access the CRBP1 binding cavity as well as its release from the cavity.

Acknowledgments

We thank the staff of beamline PXIII of Synchrotron Light Source (SLS, Villigen, Swtzerland) and of ID29 (ESRF, Grenoble, France) for technical assistance during data collection. We also thank Davide Cavazzini for valuable discussions. This work received financial support from: Universities of Padua and Parma, Italy; the European Community's Seventh Framework Program (FP7/2007-2013) under grant agreement n°283570 (for BioStruct-X); MIUR (Ministero Istruzione Universita` Ricerca) PRIN (Progetti di Rilevante Interesse Nazionale) Project 2012A7LMS3_002.

REFERENCES

Adams, P.D., Afonine, P.V., Bunkóczi, G., Chen, V.B., Davis, I.W., Echols, N., Headd, J.J., Hung, L.-W., Kapral, G.J., Grosse-Kunstleve, R.W., Mccoy, A.J., Moriarty, N.W., Oeffner, R., Read, R.J., Richardson, D.C., Richardson, J.S., Terwilliger, T.C., Zwart, P.H., 2010. PHENIX: a comprehensive Python-based system for macromolecular structure solution. Acta Crystallogr D Biol Crystallogr 66, 213–221. doi:10.1107/S0907444909052925

BOERMAN, M., NAPOLI, J.L., 1991. Cholate-Independent Retinyl Ester Hydrolysis - Stimulation by Apo-Cellular Retinol-Binding Protein. The Journal of biological chemistry 266, 22273–22278.

Boerman, M.H., NAPOLI, J.L., 1996. Cellular retinol-binding protein-supported retinoic acid synthesis. Relative roles of microsomes and cytosol. The Journal of biological chemistry 271, 5610–5616.

COWAN, S.W., NEWCOMER, M.E., JONES, T.A., 1993. Crystallographic Studies on a Family of Cellular Lipophilic Transport Proteins - Refinement of P2 Myelin Protein and the Structure Determination and Refinement of Cellular Retinol-Binding Protein in Complex with All-Trans-Retinol. Journal of Molecular Biology 230, 1225–1246. doi:10.1006/jmbi.1993.1238

Dolinsky, T.J., Nielsen, J.E., McCammon, J.A., Baker, N.A., 2004. PDB2PQR: an automated pipeline for the setup of Poisson-Boltzmann electrostatics calculations. Nucleic Acids Research 32, W665–7. doi:10.1093/nar/gkh381

Emsley, P., Cowtan, K., 2004. Coot: model-building tools for molecular graphics. Acta Crystallogr D Biol Crystallogr 60, 2126–2132. doi:10.1107/S0907444904019158

Evans, P., 2006. Scaling and assessment of data quality. Acta Crystallogr D Biol Crystallogr 62, 72–82. doi:10.1107/S0907444905036693

Folli, C., Calderone, V., Ottonello, S., Bolchi, A., Zanotti, G., Stoppini, M., Berni, R., 2001. Identification, retinoid binding, and x-ray analysis of a human retinol-binding protein. Proceedings of the National Academy of Sciences of the United States of America 98, 3710–3715. doi:10.1073/pnas.061455898

Folli, C., Calderone, V., Ramazzina, I., Zanotti, G., Berni, R., 2002. Ligand binding and structural analysis of a human putative cellular retinol-binding protein. 277, 41970–41977. doi:10.1074/jbc.M207124200

Franzoni, L., Lucke, C., Perez, C., Cavazzini, D., Rademacher, M., Ludwig, C., Spisni, A., Rossi, G.L., Ruterjans, H., 2002. Structure and backbone dynamics of apo- and holo-cellular retinol-binding protein in solution 277, 21983–21997. doi:10.1074/jbc.M201994200

Glatz, J.F., Veerkamp, J.H., 1983. A radiochemical procedure for the assay of fatty acid binding by proteins. Anal. Biochem. 132, 89–95.

Guex, N., Peitsch, M.C., 1997. SWISS-MODEL and the Swiss-PdbViewer: An environment for comparative protein modeling. Electrophoresis 18, 2714–2723. doi:10.1002/elps.1150181505

HERR, F.M., Ong, D.E., 1992. Differential Interaction of Lecithin Retinol Acyltransferase with Cellular Retinol Binding-Proteins. Biochemistry 31, 6748–6755.

Hodsdon, M.E., Cistola, D.P., 1997. Discrete backbone disorder in the nuclear magnetic resonance structure of apo intestinal fatty acid-binding protein: Implications for the mechanism of ligand entry. Biochemistry 36, 1450–1460. doi:10.1021/bi961890r

Humphrey, W., Dalke, A., Schulten, K., 1996. VMD: Visual molecular dynamics. J Mol Graph 14, 33–38.

Kabsch, W., 2010. XDS. Acta Crystallogr D Biol Crystallogr 66, 125–132. doi:10.1107/S0907444909047337

Kawaguchi, R., Zhong, M., Kassai, M., Ter-Stepanian, M., Sun, H., 2012. STRA6-Catalyzed Vitamin A Influx, Efflux, and Exchange. J. Membr. Biol. 245, 731–745. doi:10.1007/s00232-012-9463-1

Lebedev, A.A., Vagin, A.A., Murshudov, G.N., 2007. Model preparation in MOLREPand examples of model improvement using X-ray data. Acta Crystallogr D Biol Crystallogr 64, 33–39. doi:10.1107/S0907444907049839

LI, E., QIAN, S.J., WINTER, N.S., DAVIGNON, A., LEVIN, M.S., GORDON, J.I., 1991. Fluorine Nuclear-Magnetic-Resonance Analysis of the Ligand-Binding Properties of 2 Homologous Rat Cellular Retinol-Binding Proteins Expressed in Escherichia-Coli. The Journal of biological chemistry 266, 3622–3629.

Lovell, S.C., Davis, I.W., 3rd, W.B.A., de Bakker, P.I., Word, J.M., Prisant, M.G., Richardson, J.S., Richardson, D.C., 2003. Structure validation by Calpha geometry: phi,psi and Cbeta deviation. Proteins 50, 437–450.

Lu, J.Y., Lin, C.L., Tang, C.G., Ponder, J.W., Kao, J., Cistola, D.P., LI, E., 2000. Binding of retinol induces changes in rat cellular retinol-binding protein II conformation and backbone dynamics. Journal of Molecular Biology 300, 619–632. doi:10.1006/jmbi.2000.3883

Malpeli, G., Stoppini, M., Zapponi, M.C., Folli, C., Berni, R., 1995. Interactions with Retinol and Retinoids of Bovine Cellular Retinol-Binding Protein. Eur. J. Biochem. 229, 486–493.

Mittag, T., Franzoni, L., Cavazzini, D., Schaffhausen, B., Rossi, G.L., Guenther, U.L., 2006. Retinol modulates site-specific mobility of apo-cellular retinol-binding protein to promote ligand binding. J Am Chem Soc 128, 9844–9848. doi:10.1021/ja0616128

Murshudov, G.N., Skubák, P., Lebedev, A.A., Pannu, N.S., Steiner, R.A., Nicholls, R.A., Winn, M.D., Long, F., Vagin, A.A., 2011. REFMAC5 for the refinement of macromolecular crystal structures. Acta Crystallogr D Biol Crystallogr 67, 355–367. doi:10.1107/S0907444911001314

Nossoni, Z., Assar, Z., Yapici, I., Nosrati, M., Wang, W., Berbasova, T., Vasileiou, C., Borhan, B., Geiger, J., 2014. Structures of holo wild-type human cellular retinol-binding protein II (hCRBPII) bound to retinol and retinal. Acta Crystallogr D Biol Crystallogr 70, 3226–3232. doi:10.1107/S1399004714023839

Ong, D.E., MACDONALD, P.N., GUBITOSI, A.M., 1988. Esterification of Retinol in Rat-Liver - Possible Participation by Cellular Retinol-Binding Protein and Cellular Retinol-Binding Protein-Ii. The Journal of biological chemistry 263, 5789–5796.

Ong, D.E., Newcomer, M.E., Chytil, F., 1994. The retinoids: Biology, Chemistry and Medicine, in: Sporn, M.B., Roberts, A.B., Goodman, D.S. (Eds.). Raven Press, Ltd., New York, pp. 283–312.

Oostenbrink, C., Villa, A., Mark, A.E., van Gunsteren, W.F., 2004. A biomolecular force field based on the free enthalpy of hydration and solvation: The GROMOS force-field parameter sets 53A5 and 53A6. J Comput Chem 25, 1656–1676. doi:10.1002/jcc.20090

Ottonello, S., PETRUCCO, S., MARAINI, G., 1987. Vitamin-a Uptake From Retinol-Binding Protein in a Cell-Free System From Pigment Epithelial-Cells of Bovine Retina - Retinol Transfer From Plasma Retinol-Binding Protein to Cytoplasmic Retinol-Binding Protein with Retinyl-Ester Formation as the Intermediate Step. The Journal of biological chemistry 262, 3975–3981.

Ottonello, S., SCITA, G., MANTOVANI, G., Cavazzini, D., Rossi, G.L., 1993. Retinol Bound to Cellular Retinol-Binding Protein Is a Substrate for Cytosolic Retinoic Acid Synthesis. The Journal of biological chemistry 268, 27133–27142.

Randolph, T.W., 2012. The two faces of His-tag: immune response versus ease of protein purification. Biotechnol J 7, 18–19. doi:10.1002/biot.201100459

Schaap, F.G., van der Vusse, G.J., Glatz, J., 2002. Evolution of the family of intracellular lipid binding proteins in vertebrates. Mol Cell Biochem 239, 69–77.
Schuttelkopf, A.W., van Aalten, D.M., 2004. PRODRG: a tool for high-throughput crystallography of protein-ligand complexes. Acta Crystallogr D Biol Crystallogr 60, 1355–1363.
Silvaroli, J.A., Arne, J.M., Chelstowska, S., Kiser, P.D., Banerjee, S., Golczak, M., 2016. Ligand Binding Induces Conformational Changes in Human Cellular Retinol-binding Protein 1 (CRBP1) Revealed by Atomic Resolution Crystal Structures 291, 8528–8540. doi:10.1074/jbc.M116.714535
Smathers, R.L., Petersen, D.R., 2011. The human fatty acid-binding protein family: evolutionary divergences and functions. Hum. Genomics 5, 170–191. doi:10.1186/1479-7364-5-3-170
Vaezeslami, S., Mathes, E., Vasileiou, C., Borhan, B., Geiger, J.H., 2006. The structure of Apo-wild-type cellular retinoic acid binding protein II at 1.4 A and its relationship to ligand binding and nuclear translocation. Journal of Molecular Biology 363, 687–701. doi:10.1016/j.jmb.2006.08.059
van der Spoel, D., Lindahl, E., Hess, B., Groenhof, G., Mark, A.E., Berendsen, H.J.C., 2005. GROMACS: fast, flexible, and free. J Comput Chem 26, 1701–1718. doi:10.1002/jcc.20291
WINTER, N.S., BRATT, J.M., BANASZAK, L.J., 1993. Crystal-Structures of Holo and Apo-Cellular Retinol-Binding Protein-Ii. Journal of Molecular Biology 230, 1247–1259. doi:10.1006/jmbi.1993.1239
YOST, R.W., HARRISON, E.H., ROSS, A.C., 1988. Esterification by Rat-Liver Microsomes of Retinol Bound to Cellular Retinol-Binding Protein. The Journal of biological chemistry 263, 18693–18701.

Figure Captions

Fig. 1. Structures of different forms of CRBP1. (A) Cartoon view of WT holo CRBP1 with the retinol bound inside the inner cavity of the protein, showing the proximity of the retinol hydroxyl end group with the side chains of Gln-108 and Lys-40. (B) Same as (A), for CRBP1 in complex with a hypothetical fatty acid (palmitic acid). The electron density was calculated with coefficients ($2F_{obs} - F_{calc}$) and contoured at 1.5σ level. (C) Superposition of Cα chain traces of WT holo CRBP1 (chartreuse green), WT delipidated apo CRBP1 (orange), holo Q108L/K40L CRPB1 (pale cyan) and WT CRBP1 in complex with palmitic acid (raspberry). Figures 1, 2 and 3 were drawn using PyMOL (Pymol version 1.7.4, Schrödinger, LLC).

F**ig. 2. Ligand-CRBP1 interactions.** Ligand-protein interactions are shown for different forms of CRBP1**:** A) WT CRBP1-retinol complex; B) K40L CRBP1-retinol complex; C) Q108L CRBP1-retinol complex; D) CRBP1 in complex with palmitic acid (pink). In panel C), the retinol is present in two different orientations (yellow and orange), with the –OH group pointing towards either Lys40 or Met62.

Fig. 3. Molecular Dynamics simulations. RMSF values are shown for Cα atoms of WT apo CRBP1 without His-Tag (black line), with protonated His-Tag (blue line) and with unprotonated His-Tag (red line). RMSF values were calculated on the last 70 ns of MD simulations.

Fig. 4. Analysis of crystallographic B-factors. Cartoon panels showing some of the structures of CRBP1 determined here colored according to the temperature factors of the atoms, from blue (lowest) to red (highest): A) WT holo CRBP1; B) holo K40L CRBP1; C) holo Q108L CRBP1; D) holo K40L-Q108L CRBP1; E) delipidated apo CRBP1; F) apo K40L CRBP1. Secondary structure assignment was automatically performed according to PyMOL definition (The PyMOL Molecular Graphics System, Version 1.5.0.4 Schrödinger, LLC).

Fig. 5. Retinol binding assays. Representative titration curves for the interaction of retinol with WT CRBP1 (A), Q108L CRBP1 (B), K40L CRBP1 (C), and Q108L/K40L CRBP1 (D). The estimated Kd values are 4.5 nM for WT CRBP1, 64 nM for Q108L CRBP1, 71 nM for K40L CRBP1 and 255 nM for the double mutant Q108L/K40L CRBP1. For each panel the absorption spectrum of the corresponding CRBP1 form in complex with retinol is also shown. For experimental details see Materials and Methods.

Figure 1

Click here to download high resolution image

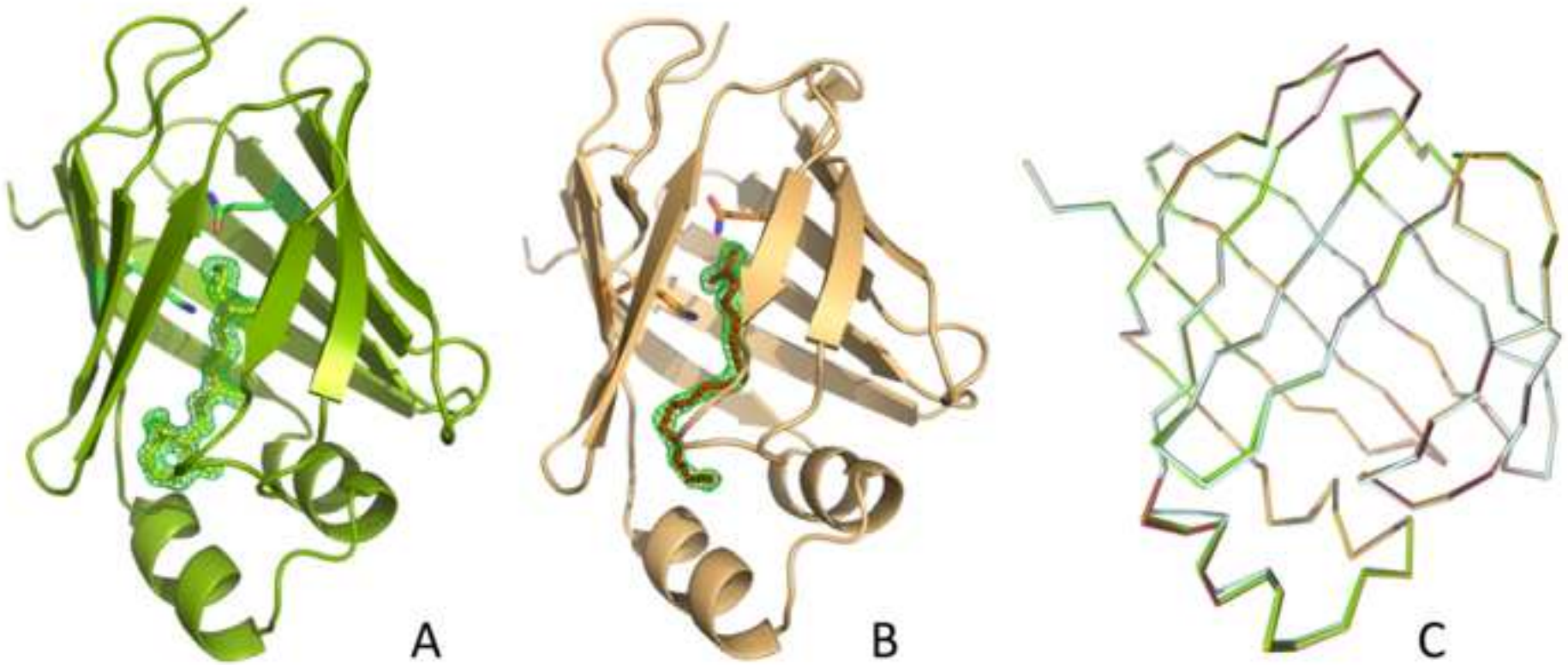

Figure 2

Click here to download high resolution image

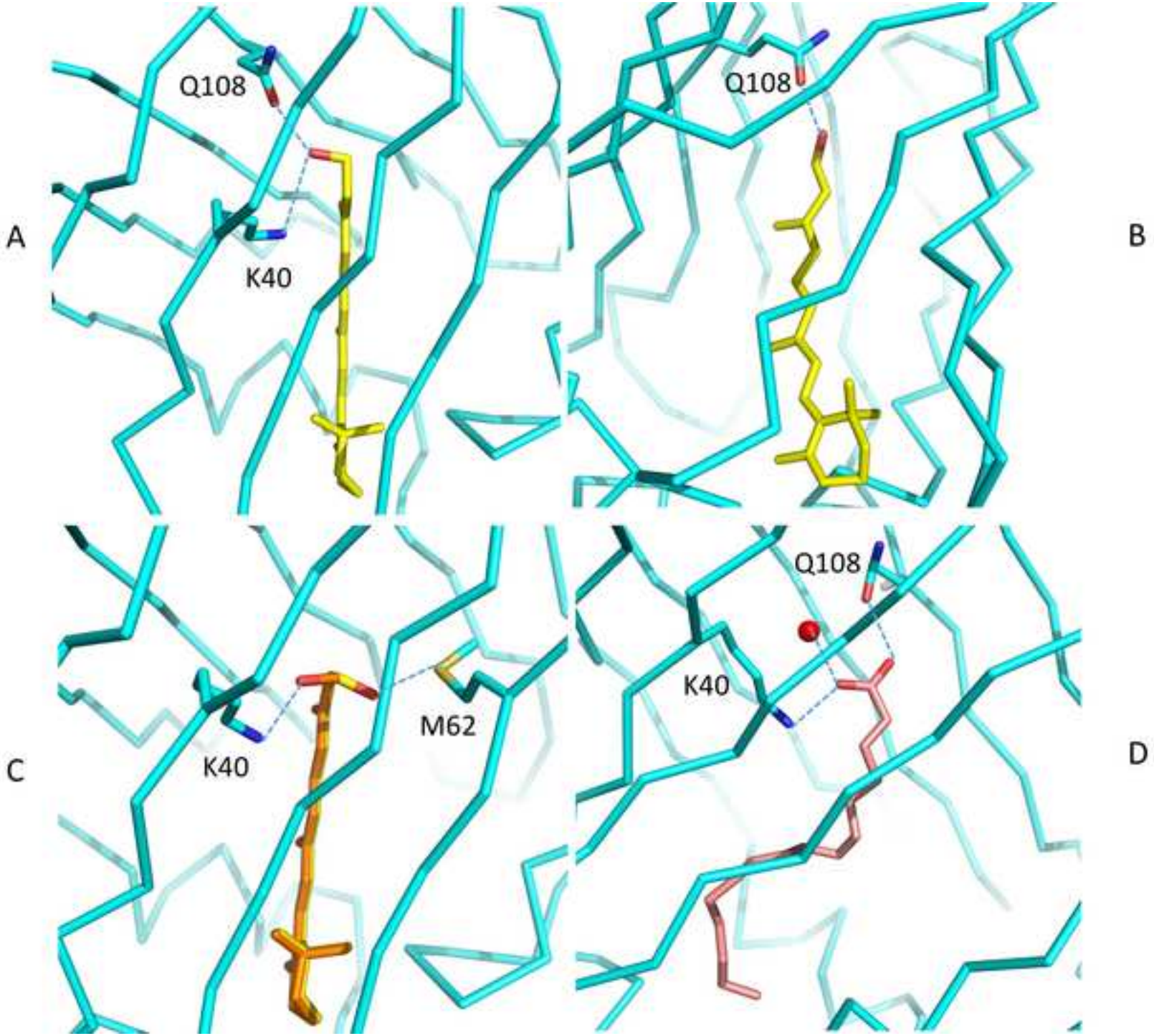

Figure 3

Click here to download high resolution image

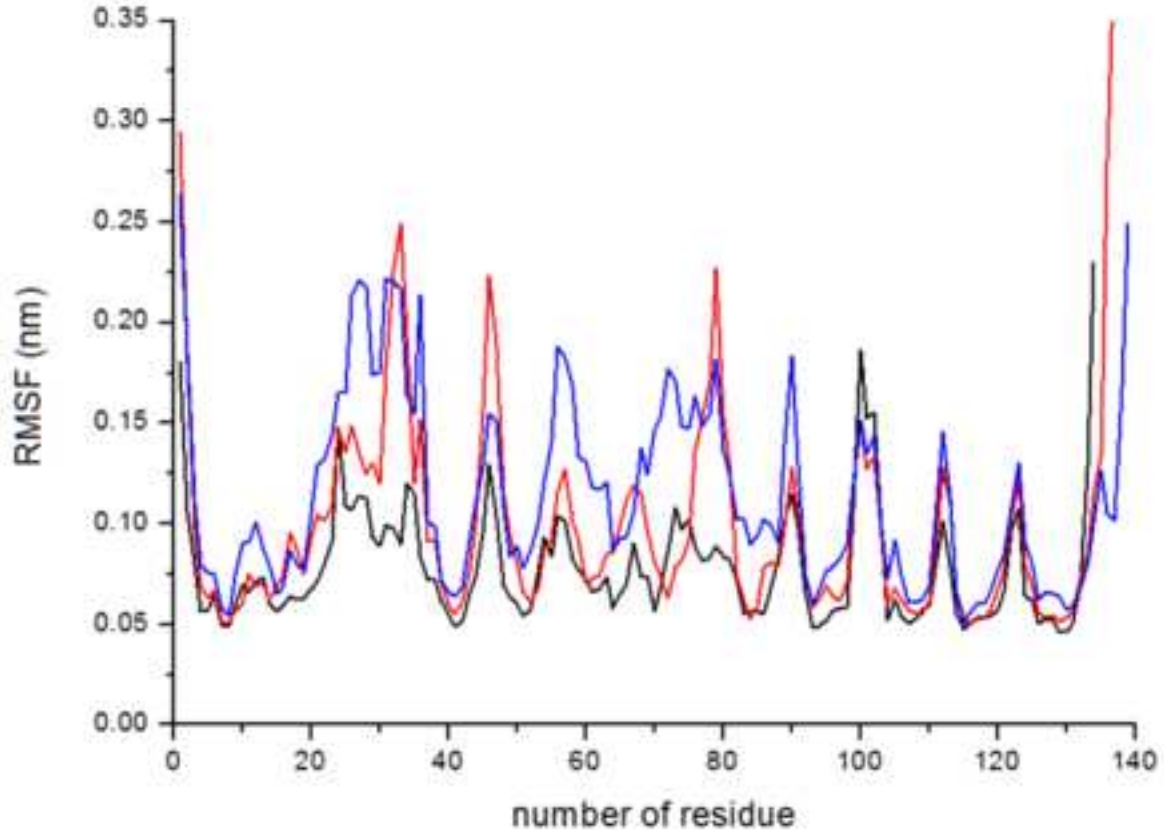

Figure 4

Click here to download high resolution image

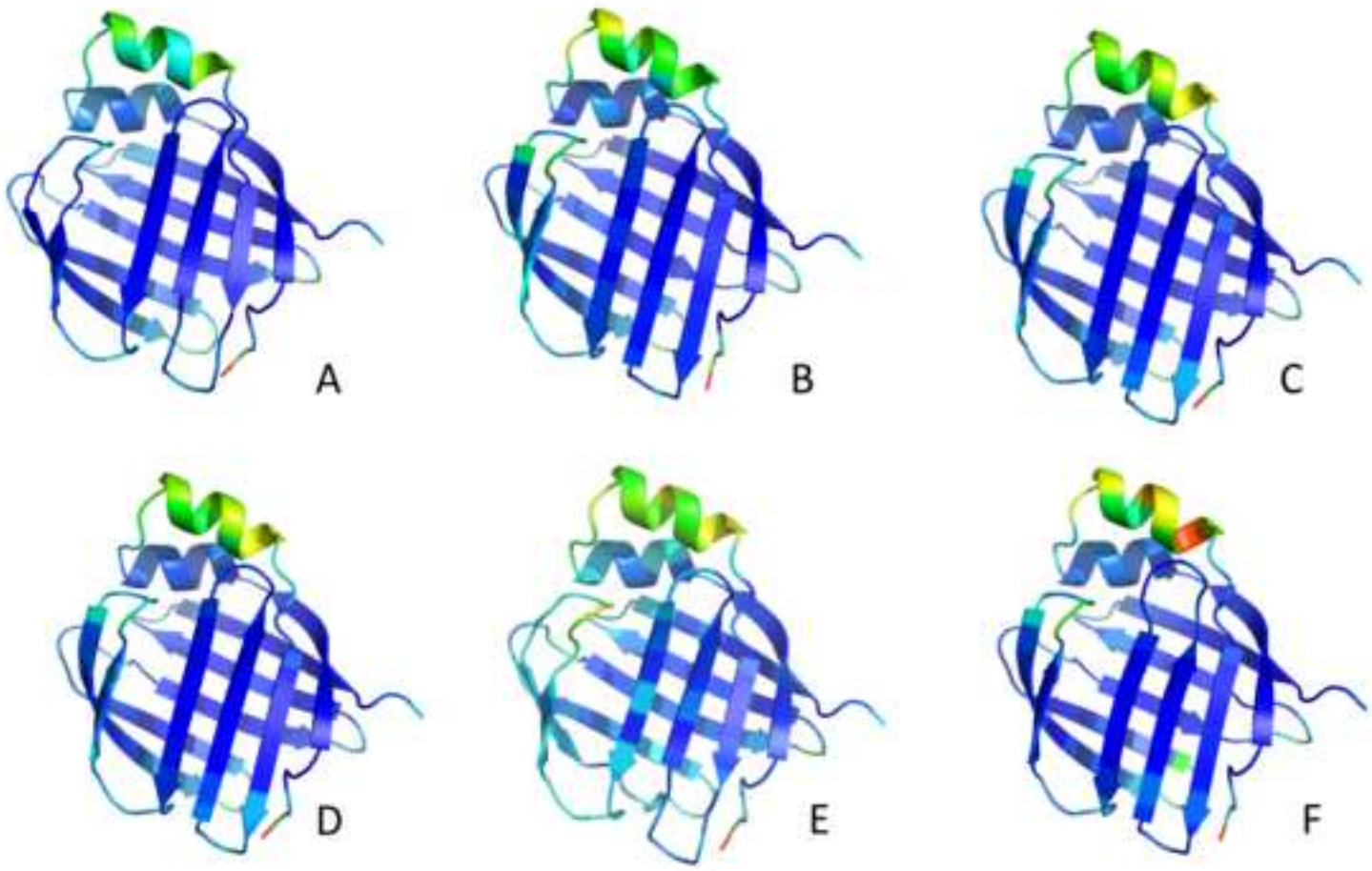

Figure 5

Click here to download high resolution image

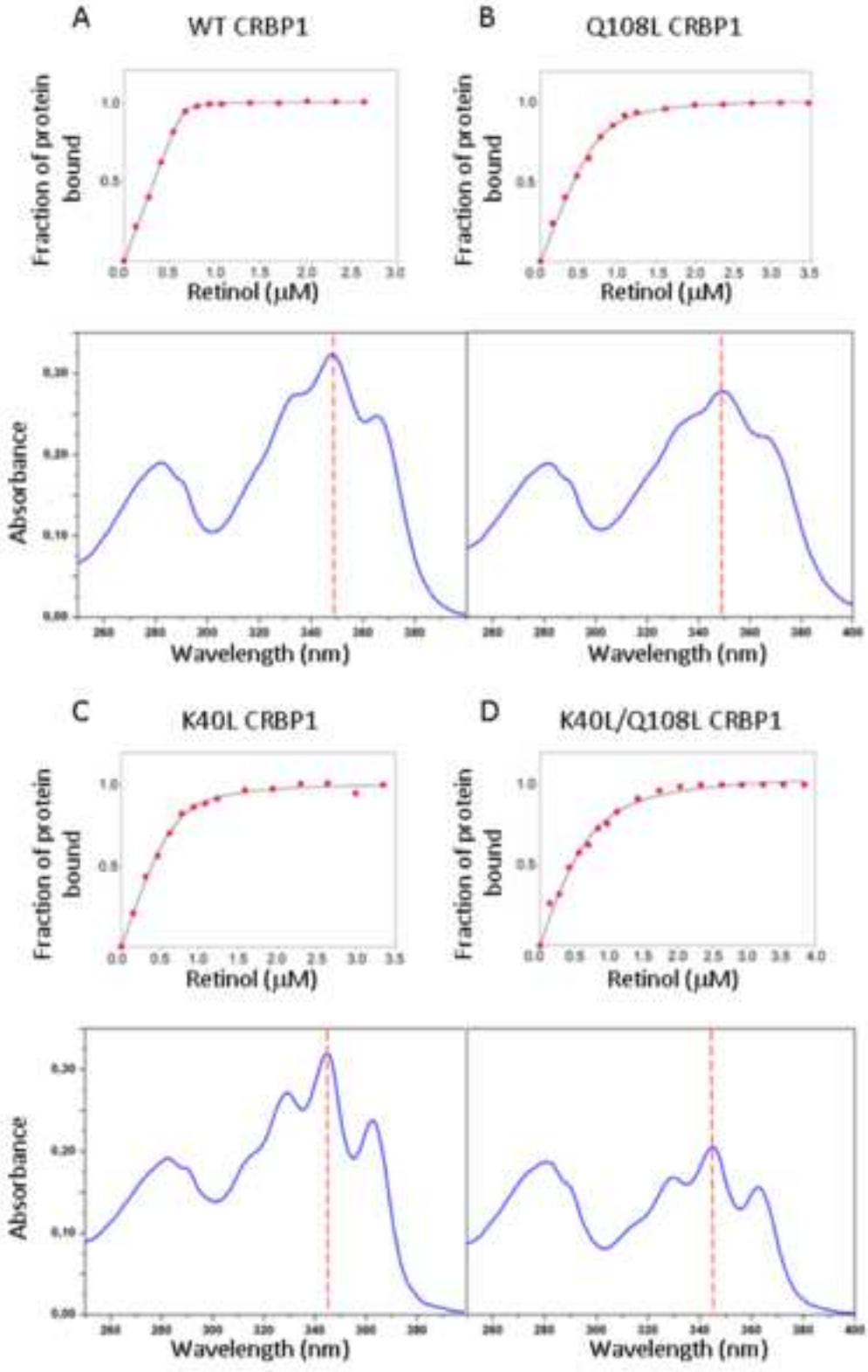

Supplemental Data - Fig. 1

Thermal motions for apo-CRBP1 structures. Cartoon structural models of delipidated WT apo CRBP1 (A) and HT apo CRBP1 (PDB ID 5H9A) (B), colored according to the temperature factors of the atoms, from blue (lowest) to red (highest).

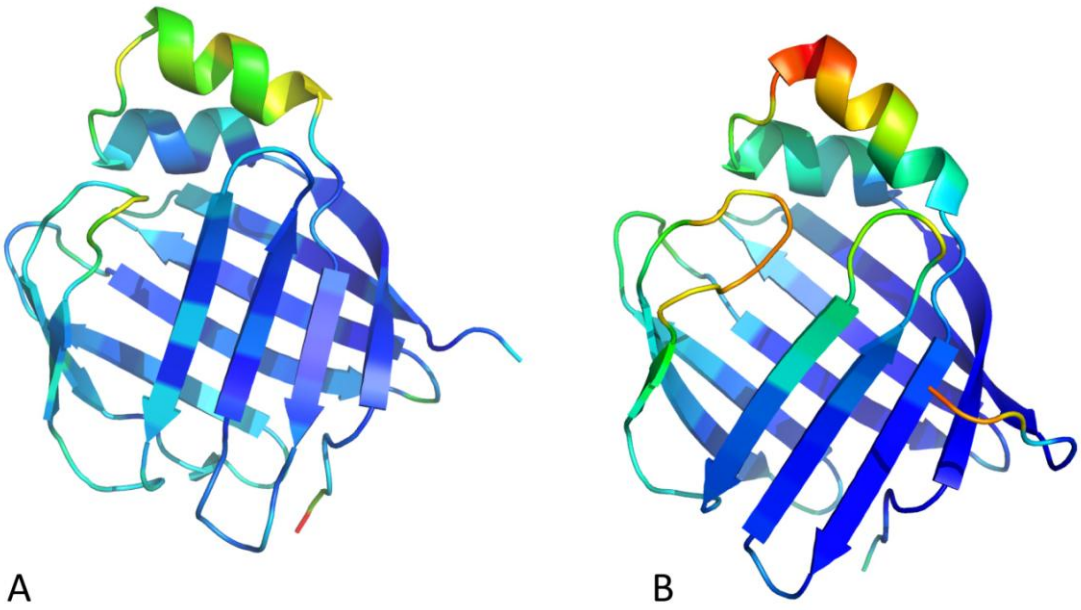

Supplemental Data - Fig. 1

Table

Table I. Statistics on data collection and refinement. 1800 frames of 0.1° each were collected. Numbers in parentheses refer to the last resolution shell.

X-ray data	Holo CRBP1	Holo CRBP1/Q108L	Holo CRBP1/K40L	Holo CRBP1/Q108L-K40L
Wavelength (Å)	0.91881	0.91881	1.000	0.91881
Space group	$P2_12_12_1$	$P2_12_12_1$	$P2_12_12_1$	$P2_12_12_1$
Cell parameters [a,b,c, Å]	34.120, 49.142, 75.801	34.035, 48.563, 75.748	34.483,47.187, 81.033	34.544, 47.414, 80.595
Resolution (Å)	41.23 – 1.26 (1.33-1.26)	40.88–1.43 (1.51–1.43)	47.19-1.61 (1.67-1.61)	47.41-1.40 (1.48-1.40)
Independent reflections	34,582 (4,718)	23,562 (2,724)	17,701 (1718)	26,769 (3,676)
Multiplicity	6.0 (5.4)	3.3 (3.0)	3.9 (4.0)	6.1 (5.7)
Completeness (%)	99.0 (94.5)	94.4 (82.5)	99.6 (99.8)	99.6 (98.1)
$<I/\sigma(I)>$	17.5 (2.9)	9.2 (2.2)	11.4 (1.6)	18.3 (2.7)
R_{merge}	0.038 (0.475)	0.063 (0.504)	0.058 (0.643)	0.043 (0.518)
R_{pim}	0.018 (0.241)	0.042 (0.293)	0.038 (0.421)	0.021 (0.255)
Refinement				
Protein atoms (no hydrogen) / solvent atoms /ligand /others	1136 / 179 / 21	1141 / 180 / 21	1107 / 195 / 21 /1	1102 / 112 /21
R_{cryst} / R_{free}	0.165 / 0.184	0.181 / 0.214	0.183 / .0234	0.194 / 0.223
Geometry				
Ramachandran favored /outliers (%)	97.0 / 0.0	97.0/0.0	97.0/ 0.0	97.0/0.0
Rotamer outliers	0.0%	0.8%		0.8%
Overall score	1.5	1.8		1.6
R.m.s.d. on bonds length [Å], angles (°)	0.011, 1.65	0.012, 1.71	0.012, 1.59	0.012, 1.57

* Completeness is low at the highest resolution, but data were left, since statistics are very good. The completeness is 99% at 1.37Å, which can be considered the actual resolution.

Table I. Continue

X-ray data	Delipidated apo CRBP1	Apo CRBP1/K40L	CRBP1-palmitic acid
Wavelength (Å)	0.973186	1.00003	0.91881
Space group	$P2_12_12_1$	$P2_12_12_1$	$P2_12_12_1$
Cell parameters [a,b,c, Å]	34.061, 47.888, 76.064	34.531, 47.603, 77.944	34.340, 48.133, 77.555
Resolution (Å)	47.89-1.70 (1.76-1.70)	47.60-1.52 (1.61-1.52)	48.13-1.15 (1.21-1.15)
Independent reflections	14,255 (1,327)	20,143 (2720)	37,927 (1,492)
Multiplicity	9.4 (6.7)	6.3 (5.8)	5.4 (2.0)
Completeness (%)	99.8 (98.5)	99.0 (93.8)	80.6 (22.4)*
$\langle I/\sigma(I)\rangle$	7.4 (0.8)	27.2 (3.2)	24.9 (3.6)
R_{merge}	0.132 (0.89)	0.031 (0.468)	0.033 (0.227)
R_{pim}	0.068 (0.663)	0.016 (0.228)	0.016 (0.170)
Refinement			
Protein atoms (no hydrogen) / solvent atoms /ligand/others	1119 / 124	1108 / 138 / 0 / 1	1129 / 234/ 18
R_{cryst} / R_{free}	0.206 / 0.251	0.171 / 0.198	0.153 / 0.173
Geometry			
Ramachandran favored / outliers (%)	97.0 / 0.0	96.2/ 0.0	96.3/ 0.0
Rotamer outliers	0.8	2.5	0.0
Overall score	1.3		1.7

RMSD on bonds length [Å], angles (°)	0.012, 1.14	0.012, 1.42	0.008, 1.24

Table II. Hydrogen bond interactions between the hydroxyl oxygen atom of retinol and protein atoms. The actual distance is reported in parentheses. In the Q108L/K40L mutant the electron density is not clear for the retinol -C_{15}–OH group, whilst the rest of the ligand is clearly visible.

CRBP1-retinol complexes	Interaction 1	Interaction 2	Electron density
WT*	Oε1 Q108 (2.92 Å)	NζK40 (3.22 Å)	Very clear for all retinol
K40L*	Oε1 Q108 (2.41 Å)	---	Very clear for all retinol
Q108L*	Sδ M62 (2.77 Å)	Nζ K40 (2.57 Å)	Reasonable density for the –OH group
Q108L/K40L**	---	---	No density for the -C_{15}–OH group

* In both WT and K40L mutant form the –OH group of retinol does not interact with any solvent molecule. In the Q108L mutant form it is present in double conformation and in each of them it interacts with a water molecule.

** In the deposited structure, although its electron density is not defined, the retinol –OH group is at 2.29 Å from Sδ of M62 and at 2.34 Å from a water molecule, well defined and held in place by three H-bonds with the carbonyl groups of Y60 and I51 and Oγ of T53.

Supplementary Material (Online Only)

Click here to download Supplementary Material (Online Only): Supplemental Data.docx